VCU

Virginia Commonwealth University
VCU Scholars Compass

Physics Publications

Dept. of Physics

2004

Competition between linear and cyclic structures in monochromium carbide clusters CrCn- and CrCn (n=2-8): A photoelectron spectroscopy and density functional study

Hua-Jin Zhai
Washington State University

Lai-Sheng Wang
Washington State University

P. Jena
Virginia Commonwealth University, pjena@vcu.edu

G. L. Gutsev
NASA Ames Research Center

C. W. Bauschlicher Jr.
NASA Ames Research Center

Follow this and additional works at: http://scholarscompass.vcu.edu/phys_pubs

Part of the Physics Commons

Competition between linear and cyclic structures in monochromium carbide clusters CrC_n^- and CrC_n ($n=2-8$): A photoelectron spectroscopy and density functional study

Hua-Jin Zhai and Lai-Sheng Wang[a)]
Department of Physics, Washington State University, Richland, Washington 99352
and W. R. Wiley Environmental Molecular Sciences Laboratory, Pacific Northwest National Laboratory,
MS K8-88, Richland, Washington 99352

P. Jena
Physics Department, Virginia Commonwealth University, Richmond, Virginia 23284-2000

G. L. Gutsev and C. W. Bauschlicher, Jr.
Mail Stop 230-3, NASA Ames Research Center, Moffett Field, California 94035

Photoelectron spectroscopy (PES) is combined with density functional theory (DFT) to study the monochromium carbide clusters CrC_n^- and CrC_n ($n=2-8$). Well-resolved PES spectra were obtained, yielding structural, electronic, and vibrational information about both the anionic and neutral clusters. Experimental evidence was observed for the coexistence of two isomers for CrC_2^-, CrC_3^-, CrC_4^-, and CrC_6^-. Sharp and well-resolved PES spectra were observed for CrC_n^- ($n=4,6,8$), whereas broad spectra were observed for CrC_5^- and CrC_7^-. Extensive DFT calculations using the generalized gradient approximation were carried out for the ground and low-lying excited states of all the CrC_n^- and CrC_n species, as well as coupled-cluster calculations for CrC_2^- and CrC_2. Theoretical electron affinities and vertical detachment energies were calculated and compared with the experimental data to help the assignment of the ground states and obtain structural information. We found that CrC_2^- and CrC_3^- each possess a close-lying cyclic and linear structure, which were both populated experimentally. For the larger CrC_n^- clusters with $n=4, 6, 8$, linear structures are the overwhelming favorite, giving rise to the sharp PES spectral features. CrC_7^- was found to have a cyclic structure. The broad PES spectra of CrC_5^- suggested a cyclic structure, whereas the DFT results predicted a linear one. © *2004 American Institute of Physics.* [DOI: 10.1063/1.1701754]

I. INTRODUCTION

Transition metals (TMs) interact with carbon in a number of ways. Early TMs form metcars[1] and carbide nanocrystals.[2] Rare-earth elements can be trapped inside fullerene cages and form endohedral metallofullerenes,[3] whereas both early TMs (e.g., Nb) (Ref. 4) and late TMs (e.g., Fe, Co, Ni, Rh, and Ir) (Ref. 5) can be substitutionally networked into fullerene cages. Late TMs are also well known for their ability to catalyze the growth of carbon nanotubes.[6] Extensive theoretical and experimental studies[7] of TM carbide clusters have been performed in the past decade to elucidate the nature of interactions between TMs and carbon.

Numerous theoretical studies have been performed on the monometal carbide MC_n series,[8–25] revealing the competition between $M-C$ and $C-C$ interactions in governing the structural evolution of the monometal carbide species. Based on the results of Hartree–Fock (HF), second-order many-body perturbation theory (MBPT[2]), and density functional theory (DFT) calculations, it has been concluded that YC_2, YC_3, YC_4, and YC_6 may possess C_{2v}, kite, fan, and linear ground-state configurations, respectively. For YC_5, both kite

and linear configurations have been found to be close in energy.[8] However, subsequent mixed HF-DFT (B3LYP) and coupled-cluster with single and double excitations (CCSD) calculations resulted in fanlike structures for both neutral YC_n ($n=3-6$) and their cations.[9] The ground states of LaC_n (up to $n=6$) were also predicted to be fan like at both B3LYP and MBPT[2] levels,[9,10] whereas larger LaC_n (up to $n=14$) were found to be cyclic with the La atom inserted into the carbon rings.[11] B3LYP calculations for TiC_n ($n=2-4$) found that the fan configurations are the most stable.[12,13] For NbC_n ($n=2-8$), extensive calculations concluded that cyclic structures are most stable, except for NbC_6, which favors a linear ground state.[14,15] Several computations performed for NiC_n showed that the relative energies of different geometrical configurations depend strongly on the level of theory applied.[16–19] Recently, DFT calculations were reported on FeC_n ($n=1-4$), concluding that all the clusters have the fanlike ground-state configurations.[20] Last, DFT calculations were also performed on late TM carbide clusters PdC_n^+ ($n=3-18$) and PtC_n^+ ($n=2-16$),[21,22] and showed that these clusters possess cyclic configurations for $n=2$, linear configurations for $n=3-9$, and again cyclic configurations for $n>10$.

Structural evolutions of several monometal TM carbide systems have also been characterized experimentally.[26–29]

————————————
a)Electronic mail: ls.wang@pnl.gov

We have used photoelectron spectroscopy (PES) to study TiC_n^- ($n=2-5$) (Ref. 26) and interpreted the vibrationally resolved PES spectra in terms of the cyclic configurations of the anions, which were confirmed by subsequent theoretical calculations.[12,13] A recent PES study of NbC_n^- ($n=2-7$) revealed experimental evidence for a cyclic-to-linear structural transition from NbC_3^- to NbC_4^- (Ref. 27). Interestingly, the PES data suggest that the Nb atom may substitute a carbon atom in the carbon chain, giving rise to linear NbC_n clusters with similar electronic properties as pure C_{n+1} clusters. For late TM systems, ion mobility experiment was carried out for FeC_n^- ($n=4-8$),[28] in which a linear isomer was observed for FeC_4^- and a two-dimensional isomer was observed for FeC_7^-, whereas both linear and two-dimensional isomers were observed for FeC_5^-, FeC_6^-, and FeC_8^-. A subsequent PES study of FeC_n^- ($n=2-5$) (Ref. 29) suggested a possible linear-to-cyclic transition from FeC_3 to FeC_4, consistent with the ion mobility measurements.

In this article, we report the results of a combined PES and DFT study on a series of monochromium carbides CrC_n^- and CrC_n ($n=2-8$). The combination of theory and experiment has proved successful in obtaining electronic and structural information about TM compound clusters.[30–33] To the best of our knowledge, previous calculations were reported only for CrC,[34–36] CrC^-,[36] and CrC^+,[37] whereas we have reported previously PES spectra for CrC_2^- and CrC_3^- in studies of the $3d$ TM MC_2^- and MC_3^- species.[38,39] The current work presents a comprehensive study on the CrC_n^- series for $n=2-8$, including CrC_2^- and CrC_3^- for completeness. Well-resolved PES spectra were obtained, providing a wealth of structural, electronic, vibrational, and isomeric information. Extensive DFT calculations using generalized gradient approximation for the exchange-correlation functional were carried out for both CrC_n and CrC_n^-. The experimental and theoretical data were combined to elucidate the electronic and structural evolution in the series.

II. EXPERIMENTAL AND COMPUTATIONAL DETAILS

A. Experimental methods

The experiments were carried out using a magnetic-bottle-type PES apparatus equipped with a laser vaporization supersonic cluster source. A detailed description of the experimental techniques can be found elsewhere.[40,41] Briefly, the CrC_n^- anions were produced by laser vaporization of a chromium carbide (Cr_3C_2) target in the presence of a helium carrier gas. Various $Cr_xC_y^-$ clusters were generated and mass analyzed using a time-of-flight mass spectrometer. The CrC_n^- ($n=2-8$) species of interest were each mass selected and decelerated before being photodetached. Three detachment photon energies were used in the current study: 532 nm (2.331 eV), 355 nm (3.496 eV), and 266 nm (4.661 eV). Photoelectrons were collected at nearly 100% efficiency by the magnetic bottle and analyzed in a 3.5-m-long electron flight tube. The photoelectron spectra were calibrated using

the known spectrum of Rh^-, and the energy resolution of the apparatus was $\Delta Ek/Ek \sim 2.5\%$—that is, ~ 25 meV for 1-eV electrons.

B. Theoretical methods

The GAUSSIAN 98 program[42] and the basis set denoted as 6-311+G*—namely, $(15s11p6d1f)/[10s7p4d1f]$ for Cr (Refs. 43–45) and $(12s6p1d)/[5s4p1d]$ for C (Ref. 46)—were used. Seven exchange-correlation functionals were tested on CrC_2 and CrC_2^-: BLYP (Becke's exchange[47] and Lee–Yang–Parr correlation[48]), BP86 (Becke's exchange[47] and Perdew's correlation[49]), BPW91 (Becke's exchange[47] and Perdew–Wang correlation[50]), PW91PW91 (both exchange and correlation are due to Perdew and Wang[50]), BPBE (Becke's exchange[47] and Perdew–Burke–Ernzerhof correlation[51]), PBEPBE (Perdew–Burke–Ezerhoff exchange and correlation[51]), and hybrid B3LYP.[52,53] Since two contenders for the ground state of CrC_2^- are close in energy at the DFT level, we also investigated the anion using the coupled-cluster singles and doubles approach[54] including the effect of connected triples determined using perturbation theory,[55] which is denoted UCCSD(T) in the MOLPRO program[56] used in this work. The $Cr(20s15p10d6f4g)/[7s6p4d3f2g]$ averaged atomic natural orbital set[57] and carbon-augmented correlation-consistent polarized valence triple-zeta (aug-cc-pVTZ) set[58,59] were used.

Only the BPW91 functional was used in the calculations for $n \geqslant 3$. Our assignment of the spectroscopic states was based on the symmetry of the Slater determinants built using the one-electron DFT orbitals. After the geometry of a species was optimized, subsequent harmonic frequency calculations were performed using analytical second derivatives in order to confirm that the optimized geometry corresponded to a minimum. Theoretical electron affinities (EAs) were obtained by the differences in total energies of a neutral and its anion at their respective equilibrium geometries (corresponding to adiabatic values):

$$EA_{ad} = E_{tot}(N, R_N) + Z_N - E_{tot}(A, R_A) - Z_A$$
$$= \Delta E_{el} + \Delta E_{nuc}, \qquad (1)$$

where R_N and R_A denote ground-state equilibrium geometries of a neutral species N and its anion A, respectively. Zero-point energies (Z) are computed within the harmonic approximation.

Vertical detachment energies (VDEs) were computed as the difference in energies between the anion ground state and the neutral state at the anion geometry:

$$VDE_k = E_{tot}(N_k, R_A) - E_{tot}(A, R_A). \qquad (2)$$

With the present approach, two VDEs corresponding to removal of an electron from the α- and β-spin orbitals can be computed—i.e., transitions to the neutral states with spin multiplicities of $2S+1 = M \pm 1$ (M stands for the spin multiplicity of an anion state) were computed.

TABLE I. Observed adiabatic (ADE) and vertical (VDE) detachment energies and vibrational frequencies for CrC_n^- ($n=2-8$). The numbers in parentheses are uncertainties in the last digits.

	Obs. feature		ADE (eV)	VDE (eV)	Vib. Freq. (cm^{-1})
CrC_2^-	X		1.617(15)	1.680 (15)	510 (20)
	A		2.011(10)	2.076 (10)	520 (20)
	B		2.30 (5)	2.36 (5)	
	C			2.466 (15)	480 (30)
	D			2.68 (3)	
	E		2.888(20)	2.888 (20)	515 (20)
	F			3.160 (10)	440 (20)
	G		3.414(10)	3.414 (10)	620 (20)
CrC_3^-	X		1.474(15)	1.474 (15)	700 (30)
	A		1.640(15)	1.640 (15)	720 (30)
	B		1.797(20)	1.797 (20)	400 (30)
	C		1.936(10)	1.936 (10)	540 (20)
	D			~2.25	
	E		2.461(20)	2.461 (20)	720 (20), 1160 (40)
	F		2.826(20)	2.826 (20)	480 (40)
	G			3.00–3.35	
CrC_4^-	X		2.781(15)	2.781 (15)	
	A	a	3.027(15)	3.027 (15)	
		b		3.063 (15)	
		c		3.102 (15)	
		d		3.144 (20)	
		e		3.186 (15)	
	B			3.35 (3)	
	C			3.55 (2)	
	D		3.88 (2)	3.94 (2)	480 (30)
	E			4.37 (2)	
	X'		~1.85	~2.05	
CrC_5^-	X		2.20 (8)	2.43 (8)	
	A			2.76 (6)	
	B			3.34 (6)	
	C			3.53 (6)	
	D			4.37 (8)	
CrC_6^-	X		3.156(10)	3.156 (10)	680 (20)
	A		3.333(10)	3.38 (2)	390 (30), 650 (20)
	B			3.61 (5)	
	C			3.69 (3)	
	D			3.92 (2)	
	X'		~2.60	~2.73	
CrC_7^-	X		2.96 (3)	3.01 (3)	
	A			3.20 (3)	
	B			~3.6	
	C			~3.9	
CrC_8^-	X		3.450(10)	3.450 (10)	
	A		3.57 (2)	3.57 (2)	970 (40)
	B			3.81 (2)	
	C			3.94 (2)	
	D			4.19 (2)	

III. EXPERIMENTAL RESULTS

The photoelectron spectra of CrC_n^- ($n=2-8$) are presented in Figs. 1–9. Figures 3 and 5 provide evidence for the existence of low-lying isomers for CrC_3^- and CrC_4^-. The adiabatic detachment energies (ADEs), VDEs, and vibrational frequencies for the resolved spectral features are given in Table I for all seven species.

A. PES spectra of CrC_2^-

Figure 1 shows the PES spectra of CrC_2^- at 532 and 355 nm. The spectra were slightly better resolved compared to those reported in our previous study.[38] In particular, hot band transitions were significantly suppressed due to our improved

ability to control cluster temperatures.[60–63] Two vibrationally resolved bands X and A were observed in the 532-nm spectrum [Fig. 1(a)]. The 0–0 transition of band X at 1.617 eV defines the ground-state ADE—i.e., EA of CrC_2. This value is more accurately measured than in our previous study, which yielded an EA of 1.63±0.01 eV for CrC_2. The VDE of band X is defined by the 1←0 transition at 1.680 eV. The well-resolved vibrational progression yielded a vibrational frequency of 510±20 cm^{-1} for the ground state of CrC_2. A similar vibrational frequency of 520±20 cm^{-1} was observed for band A. These values agree with our previous study within the experimental uncertainties.

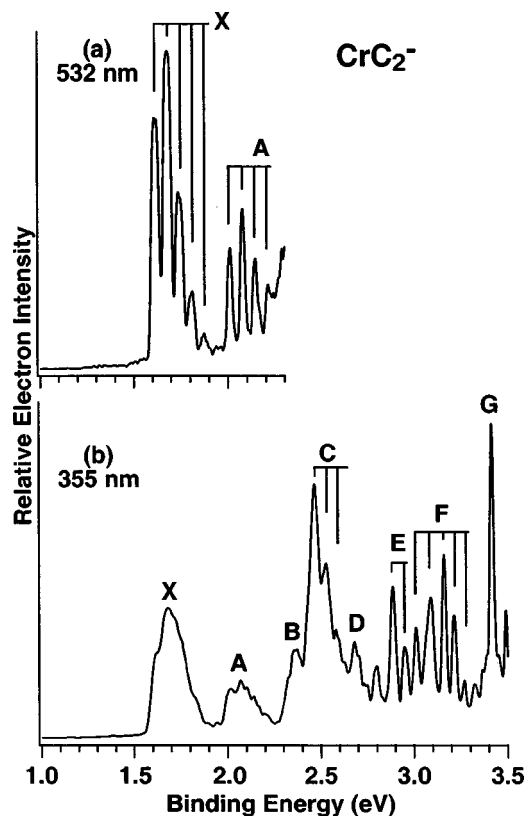A congested spectral pattern was revealed at higher bind-

FIG. 1. Photoelectron spectra of CrC_2^- at (a) 532 nm (2.331 eV) and (b) 355 nm (3.496 eV). The vertical bars indicate resolved vibrational structures.

FIG. 2. Photoelectron spectra of CrC_3^- at (a) 532 nm and (b) 355 nm.

ing energies at 355 nm [Fig. 1(b)], where numerous vibronic features were observed in the higher-binding-energy range and were tentatively labeled from B to G. Compared to our previous spectrum reported in Ref. 38, the intensity of the B band was reduced in the current colder source conditions, suggesting that this band might be due to a low-lying isomer. As will be shown later, this observation was borne out from the theoretical calculations.

B. PES spectra of CrC_3^-

The spectra of CrC_3^- are shown in Fig. 2 at 532 and 355 nm. The 532-nm spectrum [Fig. 2(a)], though better re- solved, is similar to our previous report.[39] The X, A, B, and C bands are consistent with the previous spectrum, but each with a better-resolved vibrational progression.

A congested spectrum with numerous transitions at the higher-binding-energy range was observed in the 355 nm [Fig. 2(b)], which was dominated by an extremely intense band (E) at 2.461 eV. Surprisingly, the 355-nm spectrum shown in Fig. 2(b) was quite different from the spectrum reported previously due to the colder source condition in the current experiment.[60–63] Figure 3 compares the 355-nm spec- tra of CrC_3^- taken at two different source conditions. The data in Fig. 3(a) are the same as in Fig. 2(b). The spectrum shown in Figs. 3(b) was taken at a relatively hot source con- dition, and this spectrum was similar to that reported previ- ously in Ref. 39. In addition to the deterioration of spectral resolution, dramatic intensity changes were observed. It ap-
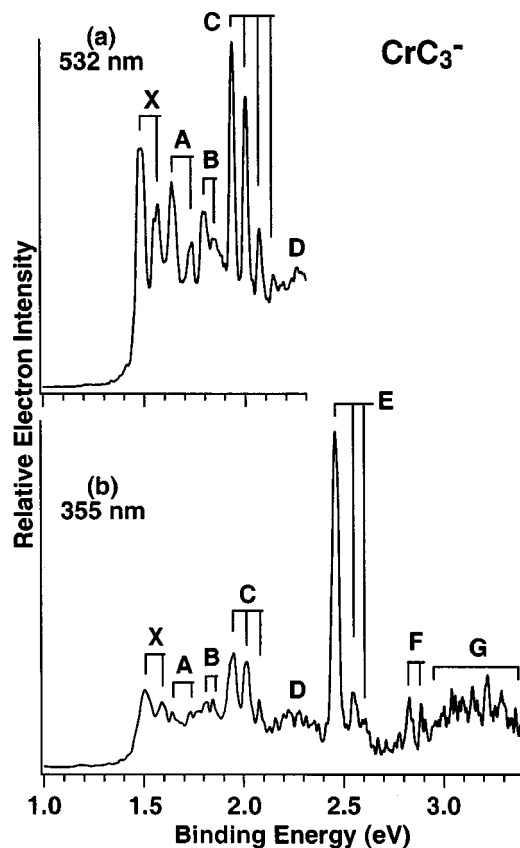
peared that the intensities of the lower- (X,A,B) and higher- (F,G) binding-energy regions were significantly enhanced relative to the central part of the spectrum (C,D,E). This observation indicates that there existed at least two low-lying isomers for CrC_3^-: one gave rise to the spectral features in the low- and high-binding-energy ranges and the other gave rise to the spectral features C, D, and E in the middle part of the 355-nm spectra (Fig. 3). The coexistence of both isomers at the colder conditions suggested that they are close in sta- bility, similar to our recent observation for B_7^- (Ref. 64).

C. PES spectra of CrC_4^-

Figure 4 shows the spectra of CrC_4^- at 355 and 266 nm. The spectra shifted significantly to higher binding energies relative to those of CrC_2^- and CrC_3^- and became much sharper and less congested. The 355-nm spectrum [Fig. 4(a)] revealed three main bands X, A, and B. Band X is sharp with little vibrational excitation, indicative of little geometry change upon photodetachment. The sharp feature X yielded an EA of 2.781 eV for CrC_4. Band A contains several re- solved fine features (a, b, c, d, and e) as shown in the inset of Fig. 4(a). The binding energies of these features are given in Table I, and they are likely due to vibrational structures for more than one electronic transition. Four more bands were observed at 266 nm, B, C, D, and E [Fig. 4(b)]. The D band consisted of a vibrational progression with a frequency of 480 cm^{-1}.

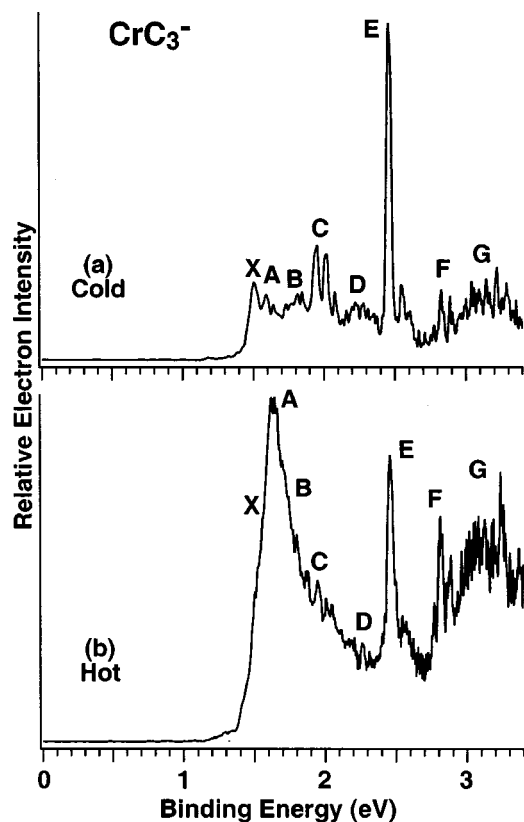A very weak band (X') was observed at the low- binding-energy side of the main features (Fig. 4). Figure 5

FIG. 3. Photoelectron spectra of CrC_3^- at 355 nm under two source conditions: (a) cold and (b) hot. Note the relative intensity changes of spectral features, indicating the coexistence of isomers in the CrC_3^- beam.
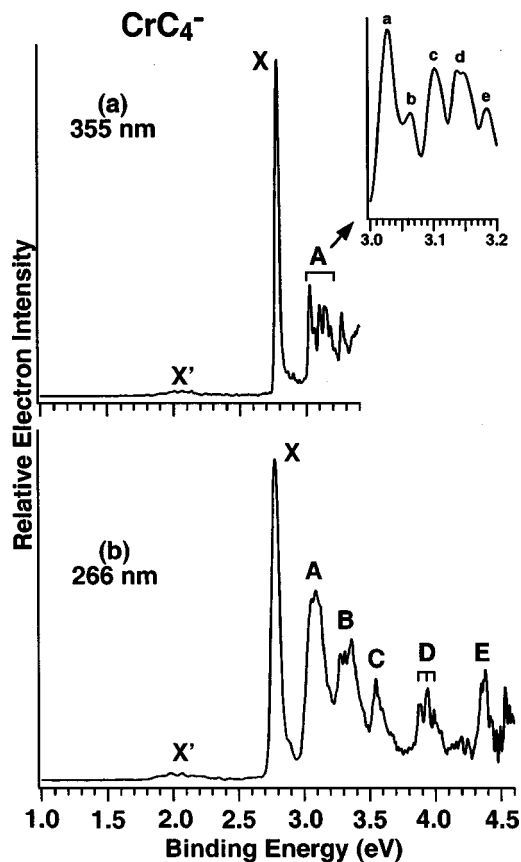

FIG. 4. Photoelectron spectra of CrC_4^- at (a) 355 nm and (b) 266 nm (4.661 eV). The inset shows fine features in band A in the 355-nm spectrum.

shows that the relative intensity of the feature X' was enhanced under hot source conditions, suggesting that it came from a higher-energy isomer. We estimated an ADE and VDE of $\sim$1.85 and $\sim$2.05 eV, respectively, for this low-lying isomer of CrC_4^-.

D. PES spectra of CrC_5^- and CrC_6^-

The spectra of CrC_5^- at 355 and 266 nm are shown in Fig. 6. These spectra represent a complete departure from those of CrC_4^-, showing extremely broad and congested features. Five bands (X, A, B, C, and D) were tentatively labeled. The ground-state VDE was estimated to be 2.43 eV, and the ADE was evaluated from the onset of feature X to be $\sim$2.2 eV. The broad spectral features suggested that there are likely large geometry changes between the anion and neutral of CrC_5.

The spectra of CrC_6^- are shown in Fig. 7 at 355 and 266 nm. These spectra are quite similar to those of CrC_4^- (Fig. 4). Analogous to that of CrC_4^-, the 355-nm spectrum of CrC_6^- [Fig. 7(a)] also exhibits two bands. The X band was sharp and intense with a short vibrational progression. The X band yielded an EA of 3.156 eV for CrC_6 and vibrational frequency of 680 cm^{-1}. The A band again consisted of several features likely due to vibrational features of more than one electronic transition. The intensity of band A increased substantially at 266 nm [Fig. 7(b)]. Three more bands were also observed at 266 nm in the higher-binding-energy range: B, C, and D. Similar to CrC_4^-, a very weak feature X' due

to a low-lying isomer was observed at the lower-binding-energy side of the main features with an ADE and VDE of $\sim$2.60 and $\sim$2.73 eV, respectively (Fig. 7).

E. PES spectra of CrC_7^- and CrC_8^-

The PES spectra of CrC_7^- are shown in Fig. 8 at 355 and 266 nm. These spectra display broad and congested features similar to those of CrC_5^-. The ground-state transition (X) was fairly well defined, yielding an EA of 2.96 eV for CrC_7. The higher-binding-energy bands (A,B,C) were tentatively identified.

The spectra of CrC_8^- are shown in Fig. 9, and they are similar to those of CrC_4^- and CrC_6^- with sharp and well-resolved PES features. The 355-nm spectrum [Fig. 9(a)] revealed only a single sharp feature X at 3.450 eV, which yielded an accurate EA of 3.450 eV for CrC_8. At 266 nm [Fig. 9(b)], four well-resolved bands (A, B, C, and D) were observed. Band A was intense and appeared to possess a partially resolved vibrational progression with a spacing of 970 cm^{-1}. The 0–0 transition of band A was broad and likely contained unresolved vibrational features corresponding to a lower-frequency mode.

The ADEs, VDEs, and vibrational frequencies for all the observed spectral features are given in Table I.
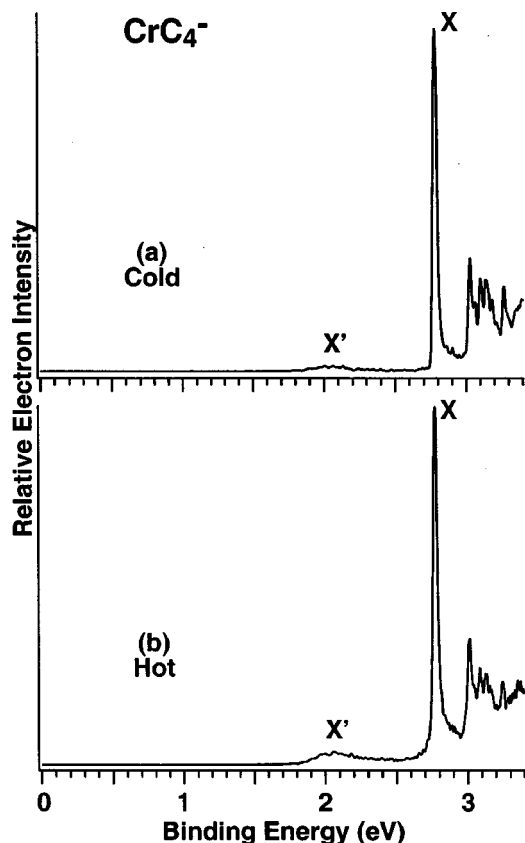
FIG. 5. Photoelectron spectra of CrC_4^- at 355 nm under two source conditions: (a) cold and (b) hot. Note the relative intensity change of feature X', indicating that this feature was due to a minor isomer of CrC_4^-.

FIG. 6. Photoelectron spectra of CrC_5^- at (a) 355 nm and (b) 266 nm.

IV. THEORETICAL RESULTS

Theoretical results at the BPW91/6-311+G* level for the neutral and negatively charged CrC_n species ($n = 2-8$) are presented in Figs. 10–16. In general, two types of structures were found: linear and cyclic (fan like). For $n = 2-4$, the local magnetic moments are also presented in order to assess changes in the spin density due to electron detachment. The local magnetic moment is defined by the differences in populations of the α- and β-spin representations. The spin densities reported in Figs. 10–12 were obtained using the conventional Mulliken analysis.[65] The differences computed using the atomic natural orbital populations[66,67] (NAOs) are essentially the same, as was noted for other systems.[68] Positive and negative values of local spin densities on carbon atoms correspond to larger populations in the α- and β-spin representations, respectively. Generally, the asymmetry in the α and β populations is small in fanlike structures, while it can reach one electron in the linear structures (Fig. 11).

A. CrC_2^- and CrC_2

We have performed an extensive search for the $n = 2$ system, including linear and nonlinear configurations. The linear CrCC structure was found to be the lowest for the CrC_2^- anion at the DFT level (Fig. 10). We paid particular attention to the nonlinear structures, including states of all possible C_{2v} symmetries, A_1, B_1, A_2, and B_2, as well as
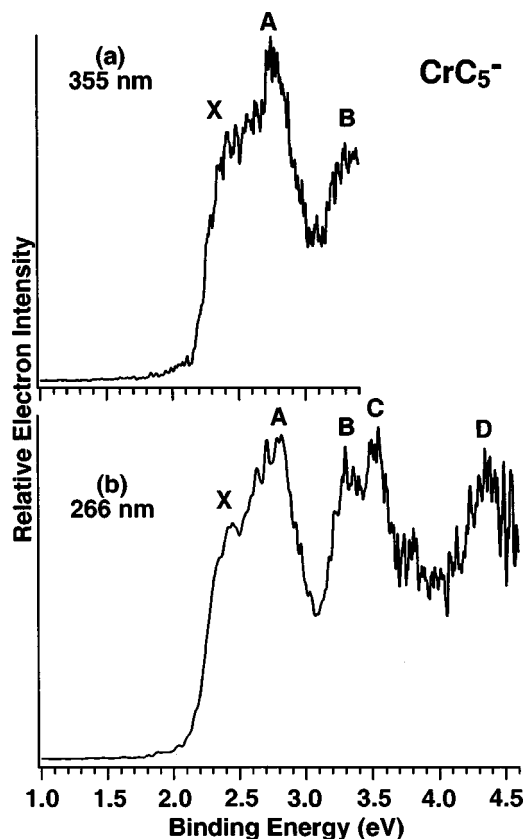
states corresponding to asymmetric angular CCrC and CrCC configurations for spin multiplicities of 4 and 6. At the BPW91 level, the lowest state found is $^6A_1$, which is above the $^6\Sigma^+$ linear state by 0.13 eV (Fig. 10). In order to make sure that this result was not an artifact of the BPW91 approach, we performed computations using six other exchange-correlation functionals, including the hybrid B3LYP functional, on the $^6\Sigma^+$ and $^6A_1$ states of CrC_2^- (Table II). We also calculated the lowest $^5A_1$ state for neutral CrC_2 at the same levels of theory, which allowed us to estimate the EA_{ad} of the C_{2v} CrC_2 at the different levels of theory. However, we found that the linear neutral CrCC was not a minimum with one imaginary frequency. In addition, calculations with the basis set extended to 6-311+G(3df) at the carbon atoms were performed. As shown in Table II, neither functional nor the basis extension influence the order of the anion states. The maximum variation in the EA_{ad} with respect to that computed at the BPW91 level was about 0.1 eV. All the approaches produced rather similar geometrical parameters and vibrational frequencies.

We also carried out CCSD(T) computations, which favored the C_{2v} $^6A_1$ state over the linear $^6\Sigma^+$ state by 0.06 eV. According to Table II, the geometrical parameters and vibrational frequencies obtained at the CCSD(T) level were in good agreement with those obtained at the DFT levels. According to the NAO analysis, the electronic configuration of Cr in the ground $^5A_1$ state of CrC_2 is $(3d^{4.34}4s^{0.33})^\alpha(3d^{0.35}4s^{0.10})^\beta$. Attachment of an extra electron leads to the lowest-energy states $^6\Sigma^+$ and $^6A_1$ of CrC_2^-. The corresponding electronic
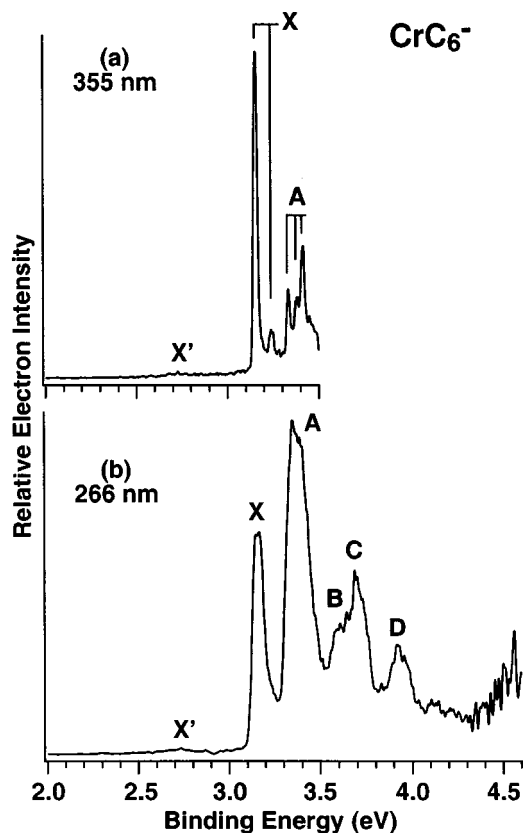
FIG. 7. Photoelectron spectra of CrC_6^- at (a) 355 nm and (b) 266 nm. The weak feature labeled X' is due to a minor isomer in CrC_6^-.

FIG. 8. Photoelectron spectra of CrC_7^- at (a) 355 nm and (b) 266 nm.

configurations are $(3d^{4.44}4s^{0.67})^\alpha(3d^{0.28}4s^{0.15})^\beta$ and $(3d^{4.56}4s^{0.78})^\alpha(3d^{0.25}4s^{0.08})^\beta$, respectively. Thus there is no substantial differences between the $^6\Sigma^+$ and $^6A_1$ NAO populations. Attachment of the extra electron substantially increases the population of the Cr $4s$ orbitals.

B. CrC_n^- and CrC_n ($n=3,4$)

As shown in Fig. 11, the fanlike ($^4B_1$) and the linear ($^4\Sigma^-$) structures of CrC_3^- were found to be nearly degenerate, with the former slightly more stable at the BPW91 level of theory. For neutral CrC_3, the low-spin ($^3B_1$) fanlike structure was the ground state with the high-spin one ($^5B_2$) being 0.15 eV higher in energy. The linear CrC_3 was higher than the $^3B_1$ structure by 0.30 eV. The electronic configuration of Cr in the ground $^3B_1$ state of CrC_3 is $(3d^{3.68}4s^{0.16})^\alpha(3d^{1.31}4s^{0.06})^\beta$. Attachment of an extra electron to CrC_3 led to $^4B_1$ of CrC_3^- with a Cr occupation of $(3d^{4.27}4s^{0.78})^\alpha(3d^{0.71}4s^{0.06})^\beta$. The electron attachment substantially increased the population of the Cr $4s$ orbitals similar to CrC_2. Note that FeC_2 and FeC_3 also possess similar cyclic structures,[23,69] although the binding patterns should be quite different since the effective configuration of an iron atom is close to $3d^74s^1$.

The ground state of CrC_4^- was found to be the linear $^6\Sigma^+$, which is well separated from the fanlike configurations (Fig. 12). However, for neutral CrC_4, the linear structure is higher than the ground-state fan structure ($^5B_2$) by 0.34 eV.
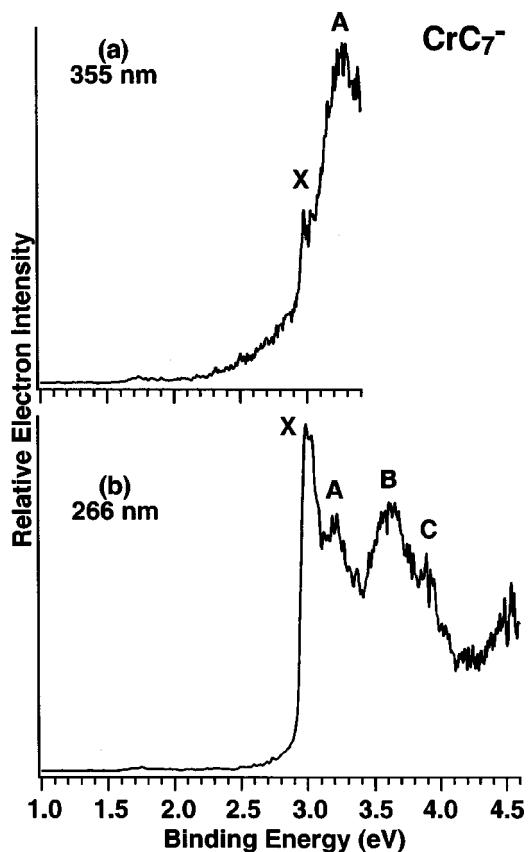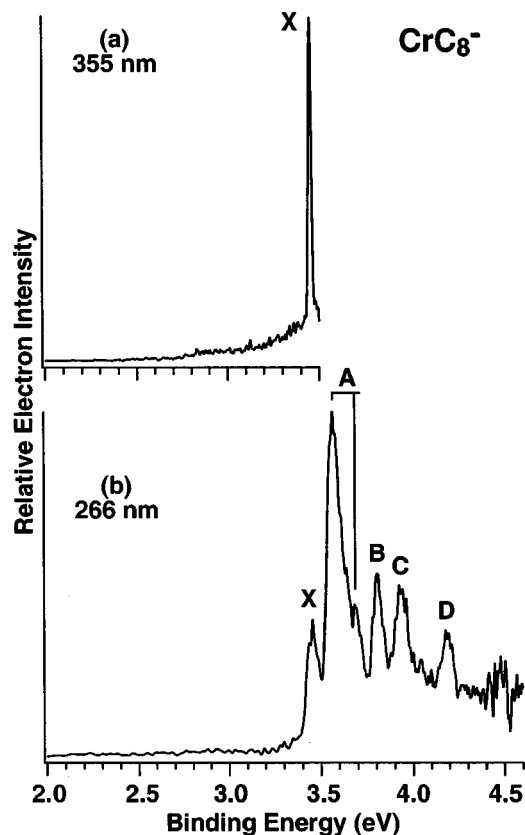
C. CrC_n^- and CrC_n ($n=5,6$)

Our BPW91 optimizations yielded a linear $^4\Sigma^-$ ground state for CrC_5^- (Fig. 13). A nonplanar fanlike structure ($^4A''$), which is 0.29 eV higher, is the lowest nonlinear structure. There are also two high-spin bent structures ($^6A'$ and $^8A''$), but they are significantly higher in energy. Neutral CrC_5 was also predicted to have a linear ground state, which is 0.16 eV below the nonplanar fanlike structure. Again, a high-spin bent CrC_7 ($^7A'$) was predicted to be 0.32 eV higher than the linear ground state. It seemed that the high-spin states prefer quasilinear configurations. We tried several starting geometries comprised of Cr on the top of or added to the side of a pentagon C_5 ring. In the first case, optimizations resulted in transition states, which finally led to the cyclic configurations found previously, while the latter converged to a cyclic $^4A''$ configuration, which is above the $^4\Sigma^-$ state by as much as 1.85 eV (Fig. 13).

Like CrC_4^-, the ground state of the CrC_6^- anion was found to be linear ($^6\Sigma^+$), which is well separated from the fan structures (Fig. 14). The closest-lying fan structure ($^4A''$) is 0.82 eV higher in energy. The neutral ground state of CrC_6 is also linear, but the fan structure ($^5A'$) is almost degenerate with the linear structure, only 0.04 eV higher. Optimizations of a configuration consisting of a Cr atom on the top of a C_6 ring led to the $^3A'$ and $^2A'$ states for the neutral and anion, respectively, as shown in Fig. 14. Both states are significantly above the ground states.

FIG. 9. Photoelectron spectra of CrC_8^- at (a) 355 nm and (b) 266 nm.

FIG. 10. Optimized structures of CrC_2 and CrC_2^- at BPW91/6-311+G*. Bond lengths are in Å and the local magnetic moments are in Bohr magnetons.

D. CrC_n^- and CrC_n ($n=7,8$)

As shown in Fig. 15, both CrC_7 and CrC_7^- were found to possess cyclic ground-state configurations corresponding to the $^3B_1$ and $^4B_1$ states, respectively. The linear structures are low-lying isomers corresponding to the $^5\Pi$ state for CrC_7 and $^4\Sigma^-$ state for CrC_7^-. The linear anion is 0.33 eV higher in energy than the cyclic ground state, but the neutral linear structure is almost degenerate with the ground state, only 0.08 eV higher. The fanlike structures are much higher in energy for both CrC_7^- and CrC_7.
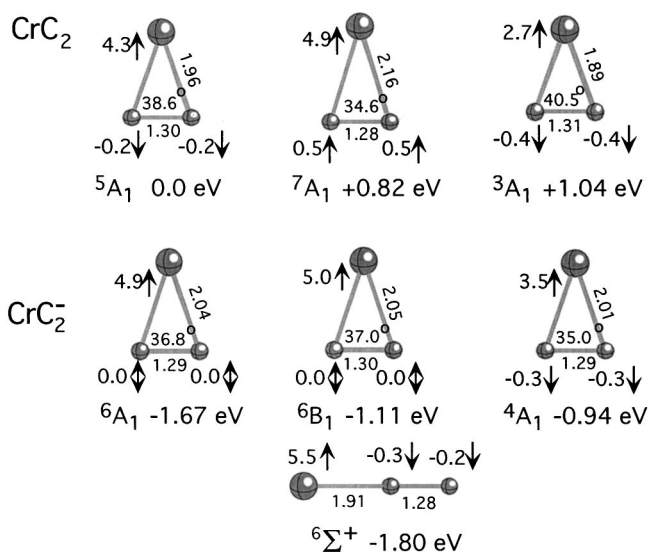
The CrC_8^- anion continues the trend of the series with an even number of carbon atoms: its ground state is linear and corresponds again to a $^6\Sigma^+$ state, while the neutral ground state is $^5\Pi$ (Fig. 16). These states are significantly more stable than the lowest cyclic states by 0.75 and 0.93 eV, respectively.

E. Theoretical EAs and VDEs

We computed the EAs for the two lowest-lying isomers for each species and the VDEs for two detachment channels (a low- and a high-spin channel). These theoretical data are given in Table III and compared with experimental data, as will be discussed below.

F. Thermodynamic stability of CrC_n and CrC_n^- clusters

In order to assess the thermodynamic stability of the monochromium carbide clusters, we evaluated the fragmentation energies of two decay channels, the loss of a C or Cr atom, as follows:

$$D_0(CrC_n^{0,-}) = E_{tot}(Cr) + E_{tot}(C_n^{0,-}) - Z(C_n^{0,-})$$
$$- E_{tot}(CrC_n^{0,-}) + Z(CrC_n^{0,-}), \quad (3)$$

$$D_0(CrC_n^{0,-}) = E_{tot}(CrC_{n-1}^{0,-}) + E_{tot}(C^{0,-})$$
$$- Z(CrC_{n-1}^{0,-}) - E_{tot}(CrC_n^{0,-})$$
$$+ Z(CrC_n^{0,-}). \quad (4)$$

The geometries of C_n and C_n^- were reoptimized at the BPW91/6-311+G* level beginning with the bond lengths taken from the B3LYP/6-311G* calculations.[70] As is well known, pure DFT approaches are biased towards overestimating the dissociation energies, by as much as 1 eV in the case of homonuclear $3d$-metal dimers.[71] If one assumes the overestimation to be nearly the same for the series of neutral and anionic species, one may compare the trends along the series.

The C_n chains possess triplet ground states for even n, which are less stable than the odd-n singlet ground-state states (see Ref. 70 and references therein). C_2 presents an exception since its singlet $^1\Sigma_g^+$ state is slightly below[72] the triplet $^3\Pi_u$ state by 0.09 eV. The BPW91 level places the triplet state of C_2 somewhat below the singlet state because it is well known[73] that it is difficult to obtain a singlet ground state of C_2 without using a multireference approach. As seen from Table IV, the even-n CrC_n species are more stable with respect to both $Cr-C_n$ and $CrC_{n-1}-C$ decay channels, although they possess higher-spin-multiplicity quintet states. The CrC_n^- anions are less stable than the corresponding neutrals with respect to the $Cr-C_n^-$ decay channel, while the large-n CrC_6^-, CrC_7^-, and CrC_8^- anions are the most stable with respect to the $CrC_{n-1}-C^-$ channel.

V. DISCUSSION

Chromium is challenging both experimentally and theoretically due to its unique half-filled $3d^5 4s^1$ electronic configuration.[74,75] The existence of structural isomers re-

TABLE II. Computational results for the $^6A_1$ and $^6\Sigma^+$ states of CrC_2^- and the $^5A_1$ of CrC_2 at different DFT-GGA levels using the 6-311+G* basis set and at CCSD(T) level.

	BLYP	BP86	BPW91	BPW91[a]	PW91*2	BPBE	PBE*2	B3LYP	CCSD(T)[b]
				Anion $^6A_1$					
r_e(Cr–C) (Å)	2.066	2.042	2.044	2.042	2.039	2.043	2.038	2.085	2.078
∠CCrC°	36.32	36.80	36.82	36.72	36.86	36.85	36.94	35.62	36.01
$\omega(b_2)$ cm^{-1}	312	334	330	331	339	331	345	289	378
$\omega(a_1)$	452	470	468	467	472	469	472	455	483
$\omega(a_1)$	1689	1686	1695	1697	1697	1692	1691	1775	1734
ΔE_{total} (eV)	**−1.59**	**−1.79**	**−1.68**	**−1.65**	**−1.72**	**−1.64**	**−1.66**	**−1.82**	**−1.58**
				Anion $^6\Sigma^+$					
r_e(Cr–C) (Å)	1.917	1.902	1.907	1.905	1.904	1.906	1.905	1.924	1.933
r_e(C–C)	1.278	1.280	1.279	1.273	1.277	1.279	1.279	1.265	1.277
$\omega(\pi)$ (cm^{-1})	174	169	169	171	171	168	169	162	140
$\omega(\sigma)$	474	482	476	477	479	476	478	488	490
$\omega(\sigma)$	1778	1780	1787	1794	1793	1786	1788	1871	1843
ΔE_{total} (eV)	**−1.72**	**−1.89**	**−1.80**	**−1.78**	**−1.81**	**−1.76**	**−1.74**	**−1.91**	**−1.52**
Neutral $^5A_1$									
r_e(Cr–C) (Å)	1.965	1.949	1.958	1.955	1.950	1.957	1.949	1.988	1.990
∠CCrC°	38.08	38.90	38.64	38.58	38.78	38.68	38.86	37.48	37.84
$\omega(b_2)$ (cm^{-1})	346	357	345	349	363	350	368	363	431
$\omega(a_1)$	505	512	497	496	510	498	510	483	520
$\omega(a_1)$	1660	1659	1673	1674	1674	1671	1669	1760	1697
ΔE_{total} (eV)	**0.0**	**0.0**	**0.0**	**0.0**	**0.0**	**0.0**	**0.0**	**0.0**	**0.0**

[a]The basis set is 6-311+G* for Cr and 6-311+G(3df) for C.
[b]The basis set is $(20s15p10d6f4g)/[7s6p4d3f2g]$ for Cr and aug-cc-pVTZ for C.

sulted in much congested PES spectra. Note, however, that photodetachment is essentially a vertical process and one-electron transitions dominate the PES spectra. Therefore, the features in the CrC_n^- spectra are primarily due to either fan-to-fan or linear-to-linear transitions. With the help of the theoretical results and temperature-dependent experimental data, it was possible to identify PES features from either linear or cyclic isomers. Our synergistic experimental and theoretical approach allowed us to obtain consistent conclusions on structural evolution in the CrC_n^- and CrC_n series.

A. CrC_2^- and CrC_2

As shown in Table II, all DFT methods predicted that the linear CrC_2^- is more stable than the cyclic isomer (Fig. 10).

But at the CCSD(T) level of theory, the cyclic structure is slightly more stable. These two isomers are likely to have similar stability and both should be populated experimentally. The calculated EA of 1.66 eV for the cyclic structure agrees well with 1.617 eV measured from the X band (Fig. 1), suggesting that the main spectral features of CrC_2^- were due to the cyclic isomer. As described in the experimental result section, the B band showed dependence on source conditions and should be due to a different isomer. The ADE estimated from the B band was 2.30 eV, which is in excellent agreement with the EA calculated for the linear to linear transition (Table III). The calculated VDEs for the two isomers are also in good agreement with the experimental val-
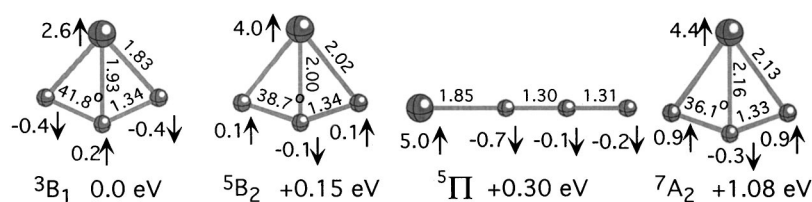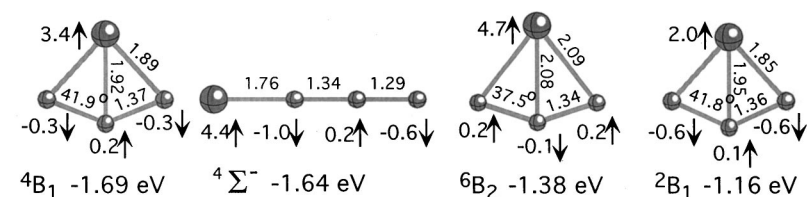

FIG. 11. Optimized structures of CrC_3 and CrC_3^- at BPW91/6-311+G*. Bond lengths are in Å and the local magnetic moments are in Bohr magnetons.
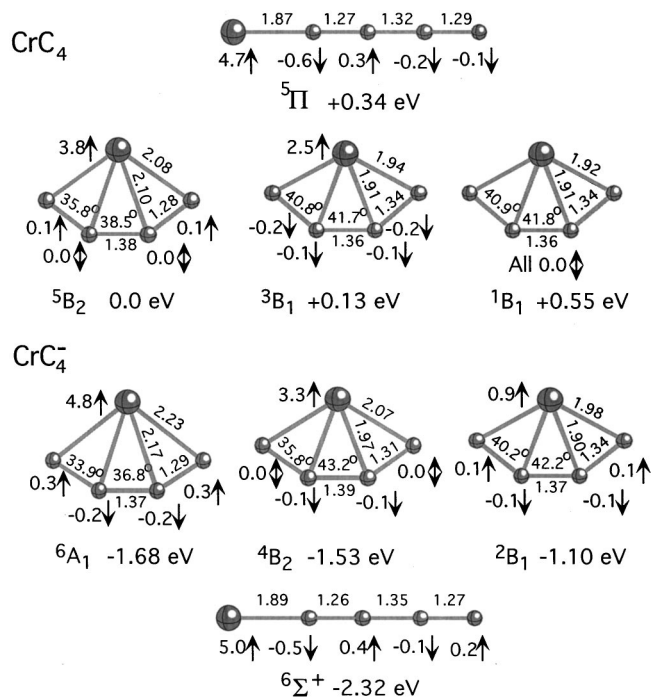
CrC$_4$

FIG. 12. Optimized structures of CrC$_4$ and CrC$_4{}^-$ at BPW91/6-311+G*. Bond lengths are in Å and the local magnetic moments are in Bohr magnetons.

CrC$_6$

FIG. 14. Optimized structures of CrC$_6$ and CrC$_6{}^-$ at BPW91/6-311+G*. Bond lengths are in Å.

ues (Table III). A high-spin excited state was also calculated for each isomer. Because of the low abundance of the linear isomer, no other spectral transitions could be identified for this isomer other than the ground-state transition. For the cy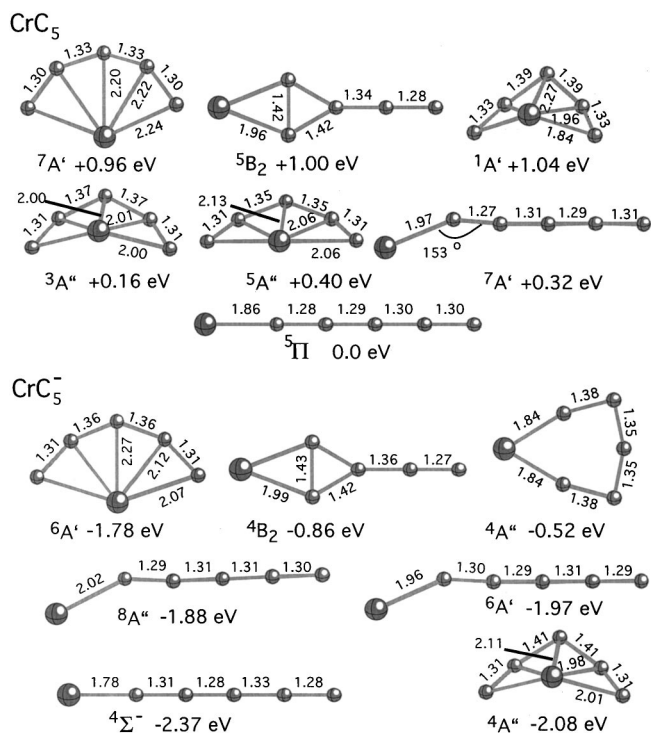clic isomer, the C band with a VDE of 2.47 eV was in good agreement with calculated VDE for the high-spin final state (Table III). Thus we conclude that the cyclic CrC$_2{}^-$ was the dominant isomer experimentally and should be the ground state, in agreement with the CCSD(T) results (Table II).

B. CrC$_3{}^-$ and CrC$_3$

Our DFT results predicted that the quartet cyclic CrC$_3{}^-$ and the linear isomer are nearly degenerate (Fig. 11). Thus they both should be populated experimentally. Figure 3 displays unambiguously the existence of two isomers in the PES spectra, as described in the Sec. III B. The calculated EA for the cyclic isomer was 1.69 eV, in reasonable agree-

CrC$_5$

FIG. 13. Optimized structures of CrC$_5$ and CrC$_5{}^-$ at BPW91/6-311+G*. Bond lengths are in Å.

CrC$_7$

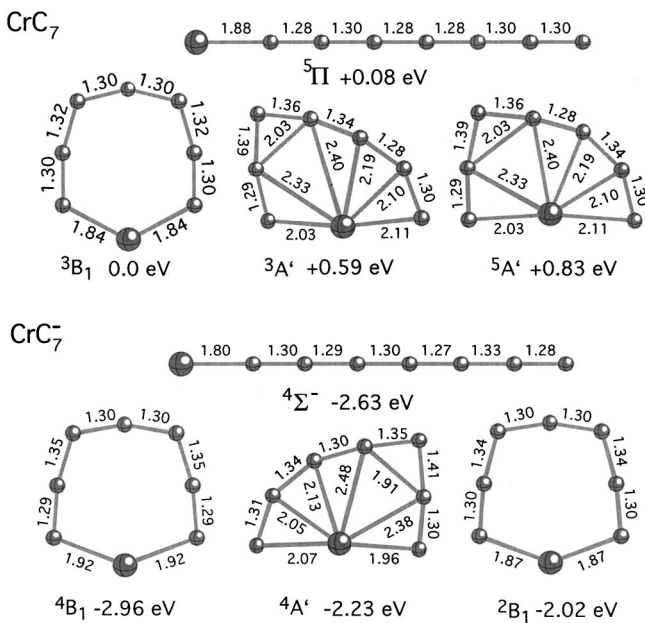FIG. 15. Optimized structures of CrC$_7$ and CrC$_7{}^-$ at BPW91/6-311+G*. Bond lengths are in Å.
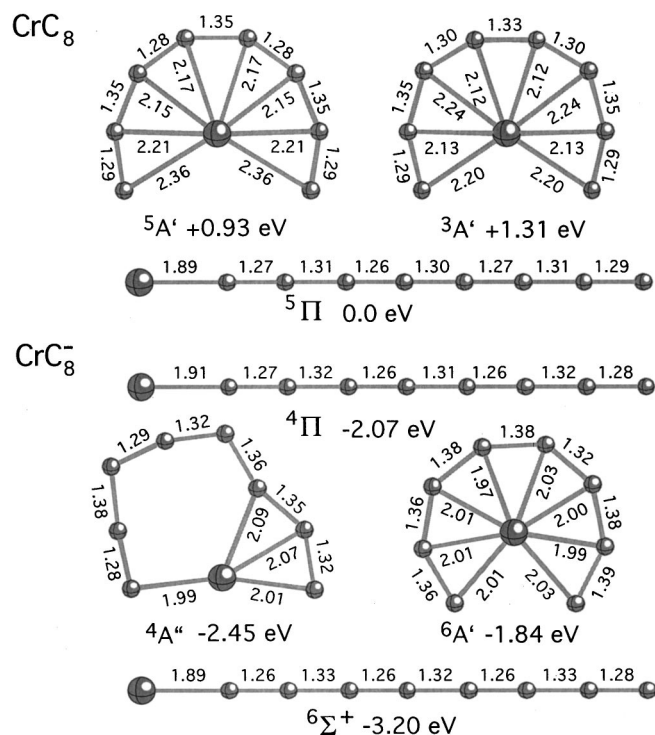
FIG. 16. Optimized structures of CrC_8 and CrC_8^- at BPW91/6-311+G*. Bond lengths are in Å.

ment with the value of 1.474 eV derived from the X band (Fig. 2). The calculated EA for the linear isomer (1.94 eV) was in excellent agreement with the value of 1.936 eV measured from the C band. Therefore, spectral features can be unambiguously identified for the two isomers on the basis of the temperature-dependent spectra shown in Fig. 3. Bands C,

D, and E were due to the linear isomer and the rest were due to the cyclic isomer. Since the abundance of the cyclic isomer increased at hotter source conditions, we conclude that the linear isomer is probably more stable than the cyclic one, although the DFT results showed that the cyclic isomer is slightly more stable (Fig. 11). We note that the agreement between the DFT results of the cyclic isomer and the experimental data is not as good as that between the DFT results of the linear isomer and the experimental data.

C. CrC_n^- and CrC_n ($n=4,6,8$)

The PES spectra for these larger even-carbon systems exhibited sharp and well-resolved data, which were different from the other spectra. Our DFT calculations predicted that all these species possess linear ground states, which are much more stable than the closest cyclic structures. Indeed, these theoretical results are in excellent agreement with our experimental observations, as shown in Table III, where the calculated EAs for the linear structures of the three species are compared with the experimental values. The sharp peak for the ground-state transitions in each case is consistent with the theoretical results that showed very little geometrical change between the anion and neutral linear structures. Even the calculated VDEs for the first excited state are in good agreement with the experimental data. Weak populations of minor isomers in the PES spectra of CrC_4^- and CrC_6^- were observed, which were in good agreement with the lowest cyclic isomers in each case. The large difference in stability between linear isomers and the cyclic ones was consistent with the extremely weak populations of the cyclic isomers in each case.

TABLE III. Comparison of experimental data with the BPW91 adiabatic electron affinities (EAs) of CrC_n and BPW91 vertical detachment energies (VDEs) from the CrC_n^-.[a]

	EA ($L^- \to L$)[b]			EA ($C^- \to C$)[c]			VDE (L^-)[d]			VDE (C^-)[e]		
		Theor.	Expt.[f]		Theor.	Expt.[f]	Final state	Theor.	Expt.[f]	Final state	Theor.	Expt.[f]
CrC_2	$^6\Sigma^+ \to {}^5\Pi$[g]	2.35	2.30 (B)	$^6A_1 \to {}^5A_1$	1.66	1.617 (X)	$^5\Pi$	2.39	2.36 (B)	$^5A_1$	1.71	1.680 (X)
							$^7\Sigma^+$	2.72		$^7A_1$	2.56	2.466 (C)
CrC_3	$^4\Sigma^- \to {}^5\Pi$	1.94	1.936 (C)	$^4B_1 \to {}^3B_1$	1.69	1.474 (X)	$^5\Pi$	2.04	1.936 (C)	$^3B_1$	1.80	1.474 (X)
							$^3\Sigma^-$	2.85	2.461 (E)	$^5B_2$	2.04	1.640 (A)
CrC_4	$^6\Sigma^+ \to {}^5\Pi$	2.65	2.781 (X)	$^6A_1 \to {}^5B_2$	1.68	~1.8 (X')	$^5\Pi$	2.69	2.781 (X)	$^5B_2$	2.07	~2.05 (X')
							$^7\Pi$	3.24	3.027 (A)	$^7A_2$	3.57	
CrC_5	$^4\Sigma^- \to {}^5\Pi$	2.37		$^4A'' \to {}^3A''$	2.23	2.20 (X)	$^5\Pi$	2.46		$^3A''$	2.43	2.43 (X)
							$^3\Pi$	3.35		$^5A''$	2.85	2.76 (A)
CrC_6	$^6\Sigma^+ \to {}^5\Pi$	2.96	3.156 (X)	$^4A'' \to {}^5A'$	2.18	~2.6 (X')	$^5\Pi$	3.00	3.156 (X)	$^5A'$	2.82	~2.73
							$^7\Pi$	3.40	3.38 (A)	$^7A''$	3.79	
CrC_7	$^4\Sigma^- \to {}^5\Pi$	2.70		$^4B_1 \to {}^3B_1$	2.96	2.96 (X)	$^5\Pi$	2.79		$^5B_2$	2.97	3.01 (X)
							$^3\Pi$	3.63		$^3B_1$	3.22	3.20 (A)
CrC_8	$^6\Sigma^+ \to {}^5\Pi$	3.20	3.450 (X)				$^5\Pi$	3.23	3.450 (X)			
							$^7\Pi$	3.54	3.57 (A)			

[a]All energies are in eV.
[b]EA for linear anion to linear neutral.
[c]EA for cyclic anion to cyclic neutral.
[d]VDE for the linear anion leading to a low and high spin final state.
[e]VDE for the cyclic anion leading to a low and high spin final state.
[f]See Table I for spectral feature assignments and uncertainties.
[g]The $^5\Pi$ state of CrC_2 has one imaginary $-287i$ cm^{-1} and corresponds to a transition state.

TABLE IV. Fragmentation energies (FEs) of CrC_n and CrC_n^- ($n = 1-8$) computed at the BPW91/6-311+G* level of theory.

Neutral		Anion	
Channel	FE (eV)	Channel	FE (eV)
$CrC^-(^3\Delta) \rightarrow Cr(^7S) + C(^3P)$	**3.50**	$CrC^-(^2\Delta) \rightarrow Cr + C^-(^4S)$	**3.43**
$CrC_2(^5A_1) \rightarrow CrC + C$	7.30	$CrC_2^-(^6\Sigma^+) \rightarrow CrC + C^-$	6.08
$\rightarrow Cr + C_2(^3\Pi_u)$	**4.30**	$\rightarrow Cr + C_2^-(^2\Sigma_g^+)$	**2.75**
$CrC_3(^3B_1) \rightarrow CrC_2 + C$	6.05	$CrC_3^-(^4B_1) \rightarrow CrC_2 + C^-$	6.37
$\rightarrow Cr + C_3(^1\Sigma_g^+)$	**2.68**	$\rightarrow Cr + C_3^-(^2\Pi_g)$	**2.28**
$CrC_4(^5B_2) \rightarrow CrC_3 + C$	6.83	$CrC_4^-(^6\Sigma^+) \rightarrow CrC_3 + C^-$	7.63
$\rightarrow Cr + C_4(^3\Sigma_g^-)$	**3.94**	$\rightarrow Cr + C_4^-(^2\Pi_g)$	**2.61**
$CrC_5(^5\Pi) \rightarrow CrC_4 + C$	6.13	$CrC_5^-(^4\Sigma^-) \rightarrow CrC_4 + C^-$	6.91
$\rightarrow Cr + C_5(^1\Sigma_g^+)$	**2.58**	$\rightarrow Cr + C_5^-(^2\Pi_u)$	**2.14**
$CrC_6(^5\Pi) \rightarrow CrC_5 + C$	6.65	$CrC_6^-(^6\Sigma^+) \rightarrow CrC_5 + C^-$	8.06
$\rightarrow Cr + C_6(^3\Sigma_g^-)$	**3.46**	$\rightarrow Cr + C_6^-(^2\Pi_u)$	**2.51**
$CrC_7(^3B_1) \rightarrow CrC_6 + C$	6.49	$CrC_7^-(^4B_1) \rightarrow CrC_6 + C^-$	7.92
$\rightarrow Cr + C_7(^1\Sigma_g^+)$	**2.78**	$\rightarrow Cr + C_7^-(^2\Pi_g)$	**2.47**
$CrC_8(^5\Pi) \rightarrow CrC_7 + C$	6.52	$CrC_8^-(^6\Sigma^+) \rightarrow CrC_7 + C^-$	8.16
$\rightarrow Cr + C_8(^3\Sigma_g^-)$	**3.34**	$\rightarrow Cr + C_8^-(^2\Pi_g)$	**2.46**

D. CrC_n^- and CrC_n ($n = 5, 7$)

In contrast to the well-resolved spectra of the even-carbon clusters, these two odd-carbon cluster species yielded very broad PES spectra, signaling that they may have very different structures or large geometry changes between their anions and neutrals. Indeed, for CrC_7^- our DFT results predicted a cyclic structure (Fig. 15) which is more stable than the linear isomer by 0.33 eV. The calculated EA and VDE for the cyclic structure are almost in perfect agreement with the experimental value (Table III). The linear isomer has a computed EA of 2.70 eV, slightly lower than the cyclic isomer. But there was no experimental evidence that this isomer was populated in any measurable amount (Fig. 8). The low-binding-energy tail in the 355-nm spectrum of CrC_7^- [Fig. 8(a)] could be due to this isomer, but this part of the spectrum was not well resolved.

The CrC_5^- and CrC_5 turned out to be the most difficult species in the series. The situation of CrC_5^- was quite unusual. Its PES spectra represented the worst resolved data among the whole CrC_n^- series. Surprisingly, our extensive DFT calculations predicted a linear ground state for CrC_5^-, which is lower in energy than the closest nonplanar cyclic structure by 0.29 eV (Fig. 13). However, the calculated EA and VDEs for the nonplanar cyclic structure are in good agreement with the experimental data (Table III), whereas the calculated EA for the linear isomer appeared to be high compared to the EA measured from the X band (Fig. 6). Thus we conclude that the main spectral features of the CrC_5^- spectra were due to the nonplanar cyclic isomer. The broad spectral transitions were consistent with the anticipated floppiness of this structure. Significant geometry changes were seen between the anion and neutral of this isomer (Fig. 13), consistent with broad PES spectral features. However, since the EA of the linear CrC_5^- isomer was calculated to be higher than the cyclic isomer, all its PES features would appear in the higher-binding-energy part of the spectra completely overlapping with those form the nonplanar cyclic iso-

mer. Thus we could not rule out a small population of the linear isomer experimentally. But this population had to be very small, because we would expect the linear isomer to give rise to more intense and sharper features dominating the PES spectra if it had a significant population, such as that observed in the spectra of CrC_3^- (Fig. 2). Thus our experimental observation suggested that CrC_5^- most likely possesses a nonlinear structure and the nonplanar cyclic one is a good candidate. In light of this apparent discrepancy, further theoretical calculations are warranted for CrC_5^- and CrC_5.

E. General remarks

The conclusions on the geometrical structures deduced from experimental observations are supported by the results of our extensive DFT calculations in terms of the relative energetics of different isomers, as well as by comparison of the ADE and VDE values presented in Table III. Discrepancies between theory and experiments were observed for CrC_5^-. We should point out that the CCSD(T) result for CrC_2^- predicted an ordering of stability for the linear and cyclic isomer different from the DFT results (Table II). A similar discrepancy between results of DFT and CCSD(T) computations was previously found for the $^4\Pi$ and $^6\Sigma^+$ states of CrO^- as well.[76] It is thus possible that a highly correlated level of theory would be needed for CrC_5^-.

Finally, it is interesting to note that the structural evolution in the CrC_n^- series is nearly identical to that found for the FeC_n^- ($n = 4-8$) series[23,28] and is similar to that observed in the NbC_n^- ($n = 2-7$) series.[27] We note that the linear CrC_n^- clusters all possess higher electron binding energies, similar to C_n^- and NbC_n^- in which linear isomers were also found to possess higher binding energies than the cyclic isomers.[27,77-79]

VI. SUMMARY

A combined anion photoelectron spectroscopy and density functional theory study on a series of monochromium carbide clusters CrC_n^- and CrC_n ($n = 2-8$) is reported. Well-resolved photoelectron spectra for CrC_n^- yielded a wealth of structural, electronic, and vibronic information. Extensive DFT calculations using the generalized gradient approximation were performed for both CrC_n^- and CrC_n series. Optimized geometries of the ground and low-lying excited states of both series were reported and compared with the experimental data. We found that the small clusters CrC_2^- and CrC_3^- possess both fanlike and linear structures with similar stability. For larger CrC_n^- clusters, the even-n species ($CrC_4^-, CrC_6^-, CrC_8^-$) exhibited sharp PES features and high binding energies and were found to possess linear structures. On the other hand, the odd-n species (CrC_5^-, CrC_7^-) displayed low binding energies and broad PES patterns and were suggested to be due to nonlinear structures. In addition to CrC_2^- and CrC_3^-, direct experimental evidence was observed for the coexistence of minor nonlinear isomers for CrC_4^- and CrC_6^-.

ACKNOWLEDGMENTS

[1] B. C. Guo, K. P. Kerns, and A. W. Castleman, Jr., Science **255**, 1411 (1992).

[2] J. S. Pilgrim and M. A. Duncan, J. Am. Chem. Soc. **115**, 9724 (1993).

[3] J. R. Heath, S. C. O'Brien, Q. Zhang, Y. Liu, R. F. Curl, H. W. Kroto, F. K. Tittel, and R. E. Smalley, J. Am. Chem. Soc. **107**, 7779 (1985).

[4] D. E. Clemmer, J. M. Hunter, K. B. Shelimov, and M. F. Jarrold, Nature (London) **372**, 248 (1994).

[5] W. Branz, I. M. L. Billas, N. Malinowski, F. Tast, M. Heinebrodt, and T. P. Martin, J. Chem. Phys. **109**, 3425 (1998).

[6] S. Iijima and T. Ichihashi, Nature (London) **363**, 603 (1993).

[7] M. M. Rohmer, M. Benard, and J. M. Poblet, Chem. Rev. **100**, 495 (2000).

[8] S. Roszak and K. Balasubramanian, J. Phys. Chem. **100**, 8254 (1996).

[9] D. L. Strout and M. B. Hall, J. Phys. Chem. **100**, 18007 (1996).

[10] S. Roszak and K. Balasubramanian, J. Phys. Chem. **106**, 158 (1997).

[11] D. L. Strout and M. B. Hall, J. Phys. Chem. A **102**, 641 (1998).

[12] R. Sumathi and M. Hendrickx, Chem. Phys. Lett. **287**, 496 (1998).

[13] R. Sumathi and M. Hendrickx, J. Phys. Chem. A **102**, 4883 (1998).

[14] D. Dai, S. Roszak, and K. Balasubramanian, J. Phys. Chem. A **104**, 5861 (2000).

[15] D. Dai, S. Roszak, and K. Balasubramanian, J. Phys. Chem. A **104**, 9760 (2000).

[16] A. N. Andriotis, M. Menon, G. E. Froudakis, and J. E. Lowther, Chem. Phys. Lett. **301**, 503 (1999).

[17] G. E. Froudakis, M. Muhlhauser, A. N. Andriotis, and M. Menon, Phys. Rev. B **64**, R241401 (2001).

[18] C. Gey, M. M. G. Alemany, O. Dieguez, and L. J. Gallego, Phys. Rev. B **62**, 12640 (2000).

[19] R. C. Longo, M. M. G. Alemany, B. Fernandez, and L. J. Gallego, Phys. Rev. B **68**, 167401 (2003).

[20] E. G. Noya, R. C. Longo, and L. J. Gallego, J. Chem. Phys. **119**, 11130 (2003).

[21] D. L. Strout, T. F. Miller III, and M. B. Hall, J. Phys. Chem. A **102**, 6307 (1998).

[22] T. F. Miller III and M. B. Hall, J. Am. Chem. Soc. **121**, 7389 (1999).

[23] A. V. Arbuznikov, M. Hendrickx, and L. G. Vanquickenborne, Chem. Phys. Lett. **310**, 515 (1999).

[24] A. V. Arbuznikov and M. Hendrickx, Chem. Phys. Lett. **320**, 575 (2000).

[25] G. Meloni, L. M. Thomson, and K. A. Gingerich, J. Chem. Phys. **115**, 4496 (2001).

[26] X. B. Wang, C. F. Ding, and L. S. Wang, J. Phys. Chem. A **101**, 7699 (1997).

[27] H. J. Zhai, S. R. Liu, X. Li, and L. S. Wang, J. Chem. Phys. **115**, 5170 (2001).

[28] G. von Helden, N. G. Gotts, P. Maitre, and M. T. Bowers, Chem. Phys. Lett. **227**, 601 (1994).

[29] L. S. Wang, Surf. Rev. Lett. **3**, 423 (1996).

[30] G. L. Gutsev, B. K. Rao, P. Jena, X. Li, and L. S. Wang, J. Chem. Phys. **113**, 1473 (2000).

[31] G. L. Gutsev, P. Jena, H. J. Zhai, and L. S. Wang, J. Chem. Phys. **115**, 7935 (2001).

[32] H. J. Zhai and L. S. Wang, J. Chem. Phys. **117**, 7882 (2002).

[33] G. L. Gutsev, C. W. Bauschlicher, Jr., H. J. Zhai, and L. S. Wang, J. Chem. Phys. **119**, 11135 (2003).

[34] I. Shim and K. A. Gingerich, Int. J. Quantum Chem. **42**, 349 (1992).

[35] R. G. A. R. Maclagan and G. E. Scuseria, J. Chem. Phys. **106**, 1491 (1997).

[36] G. L. Gutsev, L. Andrews, and C. W. Bauschlicher, Jr., Theor. Chem. Acc. **109**, 298 (2003).

[37] J. F. Harrison, J. Phys. Chem. **90**, 3313 (1986).

[38] X. Li and L. S. Wang, J. Chem. Phys. **111**, 8389 (1999).

[39] L. S. Wang and X. Li, J. Chem. Phys. **112**, 3602 (2000).

[40] L. S. Wang, H. S. Cheng, and J. Fan, J. Chem. Phys. **102**, 9480 (1995).

[41] L. S. Wang and H. Wu, in *Advances in Metal and Semiconductor Clusters*, edited by M. A. Duncan (JAI, Greenwich, 1998), Vol. 4, pp. 299–343.

[42] M. J. Frisch, G. W. Trucks, H. B. Schlegel *et al.* GAUSSIAN, Revision A.11, Gaussian, Inc., Pittsburgh, PA, 2001.

[43] A. J. H. Wachters, J. Chem. Phys. **52**, 1033 (1970).

[44] P. J. Hay, J. Chem. Phys. **66**, 4377 (1977).

[45] K. Raghavachari and G. W. Trucks, J. Chem. Phys. **91**, 1062 (1989).

[46] M. J. Frisch, J. A. Pople, and J. S. Binkley, J. Chem. Phys. **80**, 3265 (1984).

[47] A. D. Becke, Phys. Rev. A **38**, 3098 (1988).

[48] C. Lee, W. Yang, and R. G. Parr, Phys. Rev. B **37**, 785 (1988).

[49] J. P. Perdew, Phys. Rev. B **33**, 8822 (1986).

[50] J. P. Perdew and Y. Wang, Phys. Rev. B **45**, 13 244 (1992).

[51] J. P. Perdew, K. Burke, and M. Ernzerhof, Phys. Rev. Lett. **77**, 3865 (1996).

[52] A. D. Becke, J. Chem. Phys. **98**, 5648 (1993).

[53] P. J. Stevens, F. J. Devlin, C. F. Chablowski, and M. J. Frisch, J. Phys. Chem. **98**, 11623 (1994).

[54] P. J. Knowles, C. Hampel, and H.-J. Werner, J. Chem. Phys. **99**, 5219 (1993).

[55] J. D. Watts, J. Gauss, and R. J. Bartlett, J. Chem. Phys. **98**, 8718 (1993).

[56] MOLPRO is a package of *ab initio* programs written by H.-J. Werner and P. J. Knowles, with contributions from J. Almlöf, R. D. Amos, A. Berning, *et al.*

[57] C. W. Bauschlicher, Jr., Theor. Chim. Acta **92**, 183 (1995).

[58] T. H. Dunning, J. Chem. Phys. **90**, 1007 (1989).

[59] R. A. Kendall, T. H. Dunning, and R. J. Harrison, J. Chem. Phys. **96**, 6796 (1992).

[60] L. S. Wang and X. Li, in *Clusters and Nanostructure Interfaces*, edited by P. Jena, S. N. Khanna, and B. K. Rao (World Scientific, Singapore, 2000), pp. 293–300.

[61] J. Akola, M. Manninen, H. Hakkinen, U. Landman, X. Li, and L. S. Wang, Phys. Rev. B **60**, R11297 (1999).

[62] L. S. Wang, X. Li, and H. F. Zhang, Chem. Phys. **262**, 53 (2000).

[63] H. J. Zhai, L. S. Wang, A. N. Alexandrova, and A. I. Boldyrev, J. Chem. Phys. **117**, 7917 (2002).

[64] A. N. Alexandrova, A. I. Boldyrev, H. J. Zhai, and L. S. Wang, J. Phys. Chem. A, ASAP article, DOI: 10.1021/jp037341u, web release date 20 Mar 2004.

[65] R. S. Mulliken, J. Chem. Phys. **23**, 1833 (1955); **23**, 1841 (1955); **23**, 2338 (1955); **23**, 2343 (1955).

[66] A. E. Reed, R. B. Weinstock, and F. Weinhold, J. Chem. Phys. **83**, 735 (1985).

[67] A. E. Reed, L. A. Curtiss, and F. Weinhold, Chem. Rev. **88**, 899 (1988).

[68] G. L. Gutsev, L. Andrews, and C. W. Bauschlicher, Jr., J. Chem. Phys. **119**, 3681 (2003).

[69] B. K. Nash, B. K. Rao, and P. Jena, J. Chem. Phys. **105**, 11020 (1996).

[70] L. Pan, B. K. Rao, G. P. Das, and P. Ayyub, J. Chem. Phys. **119**, 7705 (2003).

[71] G. L. Gutsev and C. W. Bauschlicher, Jr., J. Phys. Chem. A **107**, 4755 (2003).

[72] K. P. Huber and G. Herzberg, *Constants of Diatomic Molecules* (Van Nostrand-Reinhold, New York, 1979).

[73] C. W. Bauschlicher, Jr. and S. R. Langhoff, J. Chem. Phys. **87**, 2919 (1987).

[74] H. Cheng and L. S. Wang, Phys. Rev. Lett. **77**, 51 (1996).

[75] L. S. Wang, H. Wu, and H. Cheng, Phys. Rev. B **55**, 12884 (1997).

[76] C. W. Bauschlicher, Jr. and G. L. Gutsev, J. Chem. Phys. **116**, 3659 (2002).

[77] S. Yang, K. J. Taylor, M. J. Craycraft, J. Conceicao, C. L. Pettiette, O. Cheshnovsky, and R. E. Smalley, Chem. Phys. Lett. **144**, 431 (1988).

[78] D. W. Arnold, S. E. Bradforth, T. N. Kitsopoulos, and D. M. Neumark, J. Chem. Phys. **95**, 8753 (1991).

[79] M. Kohno, S. Suzuki, H. Shiromaru, T. Moriwaki, and Y. Achiba, Chem. Phys. Lett. **282**, 330 (1998).